Distributed RF-Emitter Power Allocation for BiBC

Diluka Galappaththige, Fatemeh Rezaei, and Chintha Tellambura
Department of Electrical and Computer Engineering, University of Alberta, Edmonton, AB, T6G 1H9, Canada
Email: {diluka.lg, rezaeidi, ct4}@ualberta.ca

***Abstract*—In a large area such as a warehouse, using a bistatic backscatter network of passive tags for coverage brings up the issue of insufficient energy harvested by the tags, resulting in poor communication performance. To overcome this problem, we propose a solution that involves the use of distributed radio frequency emitters in a cell-free architecture to deliver more power to the tags. Our approach optimizes the emitter power allocation coefficients while ensuring the tags' energy harvesting requirements are met. By doing so, we provide the same rate quality for all tags and mitigate the effect of the tags' spatial distribution. Compared to the equal-power benchmark, our algorithm yields significant improvements. For example, it achieves $\sim 51\,\%$ and $\sim 16\,\%$ gains in harvested power and tag rate, respectively, for $0\,\mathrm{dBm}$ and $20\,\mathrm{dBm}$ with 100 emitters, respectively.**

I. Introduction

Passive Internet of Things (IoTs) networks were introduced as a potential study during the 3GPP TSG RAN meeting #94 [1], which identified several key areas and objectives:

- Use cases such as identification, tracking, monitoring, actuating, and sensing for applications in logistics, transportation, healthcare, and others.
- Exploring public/private networks, indoor/outdoor environments, macro/micro/pico cells, connectivity to user equipment (UEs) with or without relay/UE assistance, and frequency bands (both licensed and unlicensed).
- Establishing energy harvesting (EH) techniques, connectivity requirements, and positioning accuracy.

These challenges open a vast array of research questions. Very few of those have been explored [2], [3]. Inspired by them, we consider the problem of supporting multiple tags over a large coverage area such as a warehouse with a bistatic backscatter (BiBC) network of dedicated radio frequency (RF) emitters. These emit the RF signals that passive tags use for EH and reflecting back (backscatter) for data communication [2], [3]. If the passive tags do not harvest enough, they will have poor data rates and communication ranges. For instance, to wake up a sleeping tag, the incident RF power must exceed the activation threshold of around $-20\,\mathrm{dBm}$ [2]. Thus, the distance of a tag from an RF emitter must not exceed the activation distance. Thus, some tags are in energy-poor zones and may not even be activated. Consequently, not all tags achieve the same data rate.

To ease these problems, we can coordinate the RF emitters to serve multiple tags simultaneously. This requires energy beamforming at the emitters, receive filtering at the reader, and optimal power allocation to ensure uniform rates for all tags. This approach is reminiscent of distributed/cell-free massive multiple input multiple output (MIMO) wireless systems [4]. Beamforming techniques and power allocation for those have been extensively investigated with active UEs (see [4]).

Consequently, designing distributed RF emitters for BiBC with passive tags poses numerous crucial technical challenges, including (i) emitter locations, (ii) emitter power levels, (ii) beamforming strategies, (iv) power allocations to provide uniform rate, (v) minimum energy for passive tag activation, (vi) coverage, and (vii) coexistence with the conventional cellular networks. Although all these challenges in their entirety have not been investigated before, [5]–[8] address some of them. Specifically, [5], [6] explore beamforming and coexistence with a cellular network using a single-user and a single-tag system with distributed cellular access points (APs). Studies [7], [8], respectively, investigate the performance of distributed emitters in terms of coverage and capacity and their placement to maximize coverage. Except [6], no other work considers channel estimation errors account. These works assume active or semi-passive tags that may not need EH.

On the other hand, a single RF emitter is the focus of [9], [10]. Reference [9], in particular, studies the transmit power level/energy consumption at the emitter, whereas [10] investigates the emitter power allocation and energy consumption. However, tags in these systems must modify their reflection coefficients dynamically, calling for a more sophisticated tag architecture and higher power consumption.

A. Motivation and Our Contributions

The focus of this letter is different from [5]–[10]. We aim to develop a distributed RF emitter BiBC network, which can be envisioned as cell-free BiBC (Fig. 1). The design goals are to satisfy the energy requirements of the tags and preserve the basic passive tag architecture. The contributions are summarized as follows:

- We assume that the RF emitters use maximum ratio transmission (MRT) energy beamforming and the reader employs maximum ratio combining (MRC) reception. Zero-forcing (ZF) and other beamforming strategies can also be considered, although we have not included them here for brevity. Moreover, MRT is the optimal approach, as the emitters do not see interference signals.
- We also consider the impact of inter-tag interference and channel state information (CSI) errors and derive closed-form expressions for the tag rates.
- We adopt a max-min power allocation algorithm from the fractional programming techniques [11], which guarantees uniform data rates for all tags, regardless of their location or EH limitations.

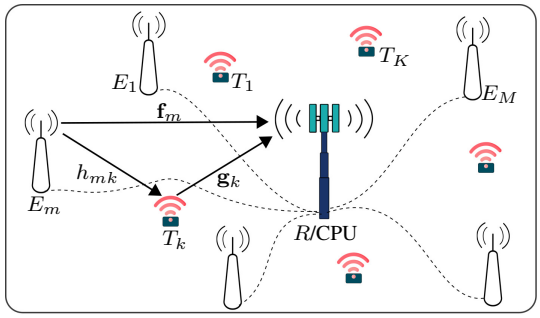

Fig. 1: Cell-free BiBC setup.

- Our analytical derivations are validated by extensive simulations. They demonstrate that utilizing distributed emitters with optimal power allocation yields significant gains. For example, for 100 emitters at $0\,\mathrm{dBm}$ and $20\,\mathrm{dBm}$, the algorithm outperforms a benchmark by $\sim 51\,\%$ in harvested power and $\sim 16\,\%$ in per-tag rate, respectively.

Note that power allocation in cell-free architecture has been extensively studied in [4, *Sec. 7*] and other references for energy/performance improvement with active UEs. However, the main difference is that our problem deals with passive tags. Unlike active UEs, passive tags entirely rely on EH without energy storage capabilities. Because the tags use passive modulation by reflection, the signal-to-interference-plus-noise ratio (SINR) expressions are different from those with active UEs. Thus, power control for BiBC networks should be developed to account for these differences.

Also, the lack of active RF components in the tags limits their processing capabilities. Thus, the goal is to simultaneously improve the harvested energy and achieved rate without changing the basic passive tag architecture, i.e., having a fixed reflection coefficient. References [7] and [8] study the performance and placement of emitters, without considering the EH constraint at tags.

Notation: Lowercase bold and uppercase bold denote vectors and matrices. A^*, $\mathbf{A}^{\mathrm{T}}$, and $\mathbf{A}^{\mathrm{H}}$, denote conjugate, transpose, and Hermitian transpose, respectively. $\mathbb{E}\{\cdot\}$ denotes the statistical expectation. Finally, $\mathcal{CN}(\boldsymbol{\mu}, \mathbf{R})$ is a complex Gaussian vector with mean $\boldsymbol{\mu}$ and co-variance matrix $\mathbf{R}$. Finally, $\mathcal{M} = \{1, \ldots, M\}$, $\mathcal{K} = \{1, \ldots, K\}$, and $\mathcal{K}_k = \mathcal{K}/k$.

II. System, Channel, and Signal Models

A. System and Channel Models

We consider a cell-free BiBC system with M single-antenna emitters, denoted by $E_m, m \in \mathcal{M}$, K single-antenna tags, denoted by $T_k, k \in \mathcal{K}$, and a L-antenna reader, denoted by R (Fig. 1). Each tag modulates its own data on the RF signals transmitted by the emitters and transmits the mixed signals to the reader. We assume that the reader comprises a central processing unit (CPU), which is connected to all emitters via an infinite capacity back-haul link [4]. Hence, this back-haul connection assists in sharing the necessary CSI between the reader and the emitters. In addition, the CPU/reader serves as the central hub that connects, controls, and coordinates all emitters and manages data transmission. The CPU's high computational capacity is also pivotal for executing optimization tasks.

The direct channels, $E_m - R$, $E_m - T_k$, and $T_k - R$ are respectively denoted by $\mathbf{f}_m \in \mathbb{C}^{L\times 1}$, $h_{mk} \in \mathbb{C}$, and $\mathbf{g}_k \in \mathbb{C}^{L\times 1}$. Moreover, $\mathbf{h}_k = [h_{1k}, \ldots, h_{Mk}]^{\mathrm{T}} \in \mathbb{C}^{M\times 1}$ denotes the effective channel between all emitters and T_k. A unified representation of all channels is given as

$$\mathbf{v} = \zeta_v^{1/2} \tilde{\mathbf{v}}, \tag{1}$$

where $\mathbf{v} \in \{\mathbf{f}_m, h_{mk}, \mathbf{g}_k\}$. In (1), ζ_v captures the large-scale path-loss and shadowing, which stays constant for several coherence intervals. Moreover, $\tilde{\mathbf{v}} \sim \mathcal{CN}(\mathbf{0}, \mathbf{I}_L)$ accounts for the small-scale Rayleigh fading[1].

CSI acquisition for the direct and backscatter channels is feasible with specially designed orthogonal pilot sequences as proposed in [12]. Because direct channels between emitters and readers are conventional cell-free one-way channels, they can be estimated more accurately, i.e. with a lower normalized mean-square error, than backscatter channels [4], [12]. In this work, we thus assume perfect CSI for direct channels. However, for the backscatter channels, we account for the imperfect CSI by modeling the channel estimation errors (Section II-A1). Moreover, estimating the cascaded channel and separating the cascaded channel into individual channels are omitted for the sake of brevity [12]. However, this will be addressed in the future extension of this work.

1) CSI Error Model: To account for channel estimation errors, we use the model

$$\mathbf{v} = \hat{\mathbf{v}} + \tilde{\mathbf{v}}, \tag{2}$$

where $\hat{\mathbf{v}} \sim \mathcal{CN}(\mathbf{0}, \delta\zeta_{\mathbf{v}}\mathbf{I}_L)$ is the channel estimate and δ ($0 \leq \delta \leq 1$) accounts for the quality of channel estimation [13]. Specifically, $\delta = 0$ and $\delta = 1$ represent no CSI and perfect CSI cases. Note that $\hat{\mathbf{v}}$ are $\tilde{\mathbf{v}}$ are uncorrelated, which indeed holds for minimum mean-square error estimation [13]. Thus, the channel estimation error can be modeled as $\tilde{\mathbf{v}} = \mathbf{v} - \hat{\mathbf{v}} \sim \mathcal{CN}(\mathbf{0}, (1-\delta)\zeta_{\mathbf{v}}\mathbf{I}_L)$ [13].

B. EH at the Passive Tag

In the considered system, tags perform EH and data transmission simultaneously via the power-splitting mode [14]. That is, T_k ($k \in \mathcal{K}$) reflects αP_k for data transmission and absorbs $P_k^{\mathrm{in}} = (1-\alpha)P_k$, for EH, where P_k is incident RF power and $\alpha \in (0, 1)$ is the reflection coefficient of the tag.

The EH circuit converts P_k^{in} to direct current power to energize the tag. The amount of harvested power at T_k, $P_{h,k}$, depends on the EH model, i.e., linear or nonlinear. In particular, for the nonlinear model, $P_{h,k} = \Phi(P_k^{\mathrm{in}})$, where $\Phi(.)$ is the nonlinear EH function [15, *Eqn. (2)*], and for the linear model, $P_{h,k} = \eta_b P_k^{\mathrm{in}}$, where $\eta_b \in (0, 1]$ is the power conversion efficiency, e.g., typical values of $\eta_b = \{0.2, 0.4, 0.6\}$ [14].

[1]Note that $h_{mk} = \zeta_{h_{mk}}^{1/2} \tilde{h}_{mk}$ and $\tilde{h}_{mk} \sim \mathcal{CN}(0, 1)$.

Regardless of the EH model, the activation threshold (p_b) of an EH circuit, i.e., the minimum power necessary to wake up the EH circuit, is a critical parameter [16]. The threshold is about $-20\,\mathrm{dBm}$ for commercial passive tags [2]. Thus, our goal is to satisfy this critical requirement for each user. In particular, our problem formulation ensures that $P_{h,k} \geq p_b$, which eventually satisfies the activation of the EH circuit. As $\Phi(x)$ is monotonically increasing function of $x \geq 0$ [15], we have $P_k^{\text{in}} \geq p_b'$, where $p_b' \triangleq \Phi^{-1}(p_b)$ for nonlinear EH model and $p_b' = p_b/\eta_b$ for linear EH case. Here, $\Phi^{-1}(p_b)$ is a constant. This reformulation thus can handle any linear or nonlinear EH model, irrespective of their properties.

C. Signal Model

The transmitted signal at E_m is given as

$$x_m = \sqrt{p_t}\sum_{i\in\mathcal{K}} \eta_{mi}^{1/2} w_{mi} s, \quad m \in \mathcal{M}, \tag{3}$$

where p_t is the transmit power at each emitter, η_{mi} is the transmit power allocation coefficient at E_m for T_i, $w_{mi} \in \mathbb{C}$ is the spatial directivity of the signal at E_m for T_k, and s is the carrier signal satisfying $\mathbb{E}\{|s|^2\} = 1$. The signal received at T_k is given as

$$y_k = \mathbf{h}_k^{\mathrm{T}}\mathbf{x} = \sqrt{p_t}\sum_{i\in\mathcal{K}} \mathbf{h}_k^{\mathrm{T}}\mathbf{N}_i^{1/2}\mathbf{w}_i s, \tag{4}$$

where $\mathbf{x} = [x_1, \ldots, x_M]^{\mathrm{T}}$, $\mathbf{N}_i = \mathrm{diag}\,(\eta_{1i}, \ldots, \eta_{Mi})$, and $\mathbf{w}_i = [w_{1i}, \ldots, w_{Mi}]^{\mathrm{T}}$. The tags must harvest enough power to support their internal operations. Hence, the input signal power at EH circuit of T_k must satisfy the following energy constraint (Section II-B):

$$P_k^{\text{in}} = (1-\alpha)|\mathbf{h}_k^{\mathrm{T}}\mathbf{x}|^2 \geq p_b'. \tag{5}$$

T_k harvests energy from the received signal and modulates it with its data, c_k, where c_k is the normalized backscatter symbol selected from a multi-level ($\bar{M}$-ary) modulation such that $\mathbb{E}\{|c_k|^2\} = 1$, before sending it to R. The received signal at R is thus given as

$$\mathbf{r} = \mathbf{F}\mathbf{x} + \sqrt{\alpha p_t}\sum_{j\in\mathcal{K}}\sum_{i\in\mathcal{K}} \mathbf{g}_j \mathbf{h}_j^{\mathrm{T}}\mathbf{N}_i^{1/2}\mathbf{w}_i s c_j + \mathbf{z}, \tag{6}$$

where $\mathbf{F} = [\mathbf{f}_1, \ldots, \mathbf{f}_M]$, $\mathbf{z} \sim \mathcal{CN}(\mathbf{0}, \sigma^2\mathbf{I}_L)$ is the additive white Gaussian noise (AWGN) vector at R.

III. Achievable Rate Analysis

The reader uses SIC to remove the direct-link signals from all emitters and then applies the detector, $\mathbf{u}_k \in \mathbb{C}^{L\times 1}$, to decode the signal of T_k. The post-processed signal for decoding T_k's data at R is thus given as

$$\begin{aligned} r_k &= \mathbf{u}_k^{\mathrm{T}}(\mathbf{r} - \mathbf{F}\mathbf{x}) \\ &= \sqrt{\alpha p_t}\mathbf{u}_k^{\mathrm{T}}\mathbf{g}_k \sum_{i\in\mathcal{K}} \mathbf{h}_k^{\mathrm{T}}\mathbf{N}_i^{1/2}\mathbf{w}_i s c_k \\ &\quad + \sqrt{\alpha p_t}\sum_{j\in\mathcal{K}_k} \mathbf{u}_k^{\mathrm{T}}\mathbf{g}_j \sum_{i\in\mathcal{K}} \mathbf{h}_j^{\mathrm{T}}\mathbf{N}_i^{1/2}\mathbf{w}_i s c_j + \mathbf{u}_k^{\mathrm{T}}\mathbf{z}. \end{aligned} \tag{7}$$

Using (7), the received SINR for T_k, γ_k, is obtained as

$$\gamma_k = \frac{\alpha p_t \left|\mathbf{u}_k^{\mathrm{T}}\mathbf{g}_k \sum_{i\in\mathcal{K}} \mathbf{h}_k^{\mathrm{T}}\mathbf{N}_i^{1/2}\mathbf{w}_i s\right|^2}{\alpha p_t \sum_{j\in\mathcal{K}_k}\left|\mathbf{u}_k^{\mathrm{T}}\mathbf{g}_j \sum_{i\in\mathcal{K}} \mathbf{h}_j^{\mathrm{T}}\mathbf{N}_i^{1/2}\mathbf{w}_i s\right|^2 + \|\mathbf{u}_k\|^2\sigma^2}. \tag{8}$$

Thus, the achievable rate of T_k at R is given as

$$\mathcal{R}_k = \mathbb{E}\{\log_2(1+\gamma_k)\} \text{ bps/Hz}. \tag{9}$$

To derive a closed-form solution of the rate in (9), we invoke [17, *Lemma 1*] and the rate is thus approximated as

$$\mathcal{R}_k \approx \log_2(1+\gamma_k') \text{ bps/Hz}, \tag{10}$$

where

$$\gamma_k' = \frac{\alpha p_t \mathbb{E}\left\{\left|\mathbf{u}_k^{\mathrm{T}}\mathbf{g}_k \sum_{i\in\mathcal{K}} \mathbf{h}_k^{\mathrm{T}}\mathbf{N}_i^{1/2}\mathbf{w}_i\right|^2\right\}}{\alpha p_t \sum\limits_{j\in\mathcal{K}_k}\mathbb{E}\left\{\left|\mathbf{u}_k^{\mathrm{T}}\mathbf{g}_j \sum\limits_{i\in\mathcal{K}} \mathbf{h}_j^{\mathrm{T}}\mathbf{N}_i^{1/2}\mathbf{w}_i s\right|^2\right\} + \mathbb{E}\{\|\mathbf{u}_k\|^2\}\sigma^2}. \tag{11}$$

Next, we assume that the emitters use MRT beamforming, and R uses MRC to receive data from tags. That is, $w_{mk} = \hat{h}_{mk}^*$ and $\mathbf{u}_k^{\mathrm{T}} = \hat{\mathbf{g}}_k^{\mathrm{H}}$ for $m \in \mathcal{M}$ and $k \in \mathcal{K}$. Hence, the closed-form of the SINR by evaluating the expectation terms in (11) is given as (12) (Appendix A).

IV. Transmit Power Control

The spatial distribution of the tags causes the near-far effect, which affects the tag's achievable rates. Nonetheless, using max-min transmit power control, which is optimal in terms of user fairness in mitigating the near-far effect [4], we can provide uniform quality of service (QoS) to all tags, as in conventional cell-free systems. To this end, for a given realization of large-scale fading, we find the power control coefficients, η_{mk} for $m \in \mathcal{M}$ and $k \in \mathcal{K}$, that maximize the minimum of all tag rates under the relevant constraints (5). This problem is thus formulated as follows:

$$\begin{aligned} \mathbf{P1}: \underset{\eta_{mk}}{\text{maximize}} \quad & \min_{k\in\mathcal{K}} \quad \mathcal{R}_k, && \text{(13a)} \\ \text{subject to} \quad & \delta\sum_{i\in\mathcal{K}} \eta_{mi}\zeta_{h_{mi}} \leq 1, \quad \text{for} \quad m \in \mathcal{M}, && \text{(13b)} \\ & (1-\alpha)\bar{P}_k \geq p_b', \quad \text{for} \quad k \in \mathcal{K}, && \text{(13c)} \\ & \eta_{mk} \geq 0, \quad \text{for} \quad m \in \mathcal{M} \text{ and } k \in \mathcal{K}, && \text{(13d)} \end{aligned}$$

where the constraint (13b) is obtained by evaluating the transmit power constraint at E_m as

$$\mathbb{E}\{|x_m|^2\} \leq p_t \Rightarrow \delta\sum_{i\in\mathcal{K}} \eta_{mi}\zeta_{h_{mi}} \leq 1. \tag{14}$$

Moreover, $\bar{P}_k$ in (13c) is the average received signal power at T_k and defined as

$$\begin{aligned} \bar{P}_k &\triangleq \mathbb{E}\{|y_k|^2\} \\ &= p_t \sum_{m\in\mathcal{M}} \left(\delta^2\eta_{mk}\zeta_{h_{mk}}^2 + \delta\sum_{i\in\mathcal{K}} \eta_{mi}\zeta_{h_{mk}}\zeta_{h_{mi}}\right). \end{aligned} \tag{15}$$

$$\gamma_k' = \frac{\alpha p_t (L+1)\zeta_{g_k}\left(\delta^2 \sum_{m\in\mathcal{M}} \eta_{mk}\zeta_{h_{mk}^2} + \delta \sum_{m\in\mathcal{M}}\sum_{i\in\mathcal{K}} \eta_{mi}\zeta_{h_{mk}}\zeta_{h_{mi}}\right)}{\alpha p_t \sum_{j\in\mathcal{K}_k}\zeta_{g_j}\left(\delta^2 \sum_{m\in\mathcal{M}} \eta_{mj}\zeta_{h_{mj}}^2 + \delta \sum_{m\in\mathcal{M}}\sum_{i\in\mathcal{K}} \eta_{mi}\zeta_{h_{mj}}\zeta_{h_{mi}}\right) + \sigma^2} \tag{12}$$

Since $\mathcal{R}_k$ is a monotonically increasing function of γ_k', we can replace it with γ_k'. Thereby, $\mathbf{P1}$ is reformulated as [11]

$$\mathbf{P2}: \underset{\boldsymbol{\eta}}{\text{maximize}} \ \min_{k\in\mathcal{K}} \ \frac{A_k(\boldsymbol{\eta})}{B_k(\boldsymbol{\eta})}, \tag{16a}$$

$$\text{subject to } \delta \sum_{i\in\mathcal{K}} \eta_{mi}^2 \zeta_{h_{mi}} \le 1, \quad \text{for} \quad m \in \mathcal{M}, \tag{16b}$$

$$(1-\alpha)\bar{P}_k \ge p_b', \quad \text{for} \quad k \in \mathcal{K}, \tag{16c}$$

$$\eta_{mk} \ge 0, \quad \text{for} \quad m \in \mathcal{M} \text{ and } k \in \mathcal{K}, \tag{16d}$$

where $\boldsymbol{\eta} = [\eta_{11}, \ldots, \eta_{MK}]^{\mathrm{T}}$. Besides, $A_k(\boldsymbol{\eta})$ and $B_k(\boldsymbol{\eta})$ are the numerators and denominators of the corresponding SINR terms γ_k' (12). Next, by defining a common SINR, λ, for all tags, and invoking quadratic transform technique [11], $\mathbf{P2}$ is equivalent to

$$\mathbf{P3}: \underset{\boldsymbol{\eta}}{\text{maximize}} \ \lambda, \tag{17a}$$

$$\text{subject to } \delta \sum_{i\in\mathcal{K}} \eta_{mi}^2 \zeta_{h_{mi}} \le 1, \quad \text{for} \quad m \in \mathcal{M}, \tag{17b}$$

$$(1-\alpha)\bar{P}_k^{\mathrm{Lin}} \ge p_b', \quad \text{for} \quad k \in \mathcal{K}, \tag{17c}$$

$$\eta_{mk} \ge 0, \quad \text{for} \quad m \in \mathcal{M} \text{ and } k \in \mathcal{K}, \tag{17d}$$

$$2q_k\sqrt{A_k(\boldsymbol{\eta})} - q_k^2 B_k(\boldsymbol{\eta}) \ge \lambda, \tag{17e}$$

where $\mathbf{q} = [q_1, \ldots, q_K]^{\mathrm{T}}$ is the auxiliary variable introduced by the quadratic transform [11]. For a fixed $\boldsymbol{\eta}$, the optimal q_k is given in closed-form as

$$q_k^\star = \sqrt{A_k(\boldsymbol{\eta})}/B_k(\boldsymbol{\eta}), \quad \text{for} \quad k \in \mathcal{K}. \tag{18}$$

Moreover, $\bar{P}_k^{\mathrm{Lin}}$ is the linearized received signal power at T_k. It is obtained by applying Taylor series linearization techniques. Thus, $\bar{P}_k^{\mathrm{Lin}} = p_t \hat{P}_k^{\mathrm{Lin}}$, and $\hat{P}_k^{\mathrm{Lin}}$ is given as

$$\begin{aligned}\hat{P}_k^{\mathrm{Lin}} = &\sum_{m\in\mathcal{M}}\left(\delta^2 \eta_{mk}^{(t-1)}\zeta_{h_{mk}}^2 + \delta\sum_{i\in\mathcal{K}}\eta_{mk}^{(t-1)}\zeta_{h_{mk}}\zeta_{h_{mi}}\right)\\ &+\delta(\delta+1)\sum_{m\in\mathcal{M}}\zeta_{h_{mk}}^2\left(\eta_{mk}^{(t)} - \eta_{mk}^{(t-1)}\right)\\ &+\delta\sum_{m\in\mathcal{M}}\sum_{i\in\mathcal{K}}\zeta_{h_{mk}}\zeta_{h_{mi}}\left(\eta_{mk}^{(t)} - \eta_{mk}^{(t-1)}\right),\end{aligned} \tag{19}$$

where $\eta_{mk}^{(t)}$ and $\eta_{mk}^{(t-1)}$ are current and previous values of η_{mk}.

For fixed $\mathbf{q}$, due to the concavity of each $A_k(\boldsymbol{\eta})$, the convexity of each $B_k(\boldsymbol{\eta})$, and that the square-root function is concave and increasing, the quadratic transformed constraint (17e) is concave in $\mathbf{P3}$. Hence, $\mathbf{P3}$ is a concave maximization problem over $\boldsymbol{\eta}$ for fixed $\mathbf{q}$. Thus, convex algorithms can efficiently obtain optimal $\boldsymbol{\eta}$. Algorithm 1 gives the details.

Remark 1. *Algorithm 1 describes the proposed optimization methods for solving $\boldsymbol{\eta}$. It begins by setting $\boldsymbol{\eta}$ to a random feasible value, and then in each iteration, $\boldsymbol{\eta}$ is improved by computing $\mathbf{q}$. This continues until the objective stops increasing, i.e., the common rate increment is less than $\epsilon = 10^{-3}$.*

Algorithm 1 : Transmit power control.

Initialization: Initialize $\boldsymbol{\eta}$ to a feasible value. Set $\eta_{mk}^{(0)} = 1/\sqrt{K}$ for $m \in \mathcal{M}$ and $k \in \mathcal{K}$. Replace each $A_k(\boldsymbol{\eta})/B_k(\boldsymbol{\eta})$ with $2q_k\sqrt{A_k(\boldsymbol{\eta})} - q_k^2 B_k(\boldsymbol{\eta})$.

Repeat

Step 1: Update $\mathbf{q}$ by (18).

Step 2: Update $\boldsymbol{\eta}$ by solving $\mathbf{P3}$ for fixed $\mathbf{q}$.

Until convergence.

Output: η_{mk} for $m \in \mathcal{M}$ and $k \in \mathcal{K}$.

Remark 2. *In $\mathbf{P1}$, we consider fixed reflection coefficients at the tags, α_k, to keep the tags' power, cost, and form factor to a minimum [18]. However, α_k's can be optimized at the expense of a simple tag architecture. Since $\boldsymbol{\eta}$ and α_k's are independent variables, we can utilize alternative optimization to find the optimal $\boldsymbol{\eta}$ and α_k's. We will address this in the future extension of this work.*

A. Computational Complexity

The proposed max-min optimization for obtaining the transmit power control coefficient is a multistage iterative algorithm, i.e., Algorithm 1, which is developed utilizing fractional programming. The outer loop, in particular, is accountable for optimizing $\boldsymbol{\eta}$ (Step 2 in Algorithm 1), while the inner loop is accountable for updating the auxiliary variable $\mathbf{q}$ (Step 1 in Algorithm 1), introduced by fractional programming approaches. Since $\mathbf{q}$ is obtained in closed-form (18), the computational complexity of Algorithm 1 lies in step 2. In addition, CVX Matlab handles this optimization problem with an SDPT3 solver. Therefore, the computational complexity of Algorithm 1 is $\mathcal{O}(K^3M^3L^3)$ [19], [20]. As a result, the proposed approach for the max-min optimization has a total complexity of $\mathcal{O}(I_t K^3 M^3 L^3)$, where I_t is the number of iterations of Algorithm 1.

V. Simulation Results

This section gives several system simulations. We adopt the 3GPP UMi model for the large-scale fading ζ_v with $f_c = 3\,\mathrm{GHz}$ operating frequency [21, Table B.1.2.1]. Moreover, the AWGN variance is set at $\sigma^2 = 10\log_{10}(N_0 B N_f)\,\mathrm{dBm}$, where $N_0 = -174\,\mathrm{dBm/Hz}$, B is the bandwidth, and N_f is the noise figure. To model the coverage area, e.g., warehouse, we consider a $100 \times 100\ \mathrm{m}^2$ square area, the reader is located at the center, the emitters are uniformly distributed, and the tags are randomly distributed within the area. Unless otherwise specified, Table I gives the simulation parameters.

TABLE I: Simulation settings.

Parameter	Value	Parameter	Value
B	10 MHz	L	4
N_f	10 dB	K	3
α	0.6	δ	1
M	32	p_b	-20 dBm

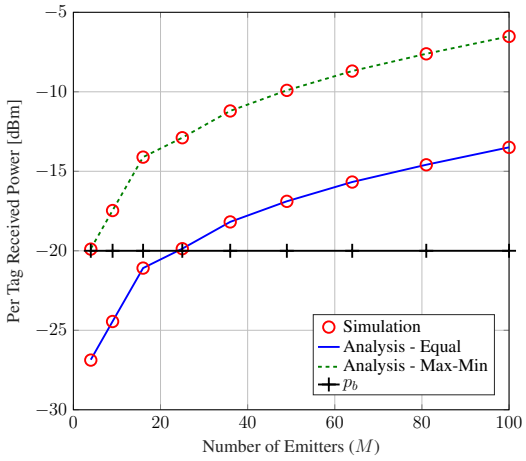

Fig. 2: Per tag received power versus the number of emitters for $p_t = 0$ dBm.

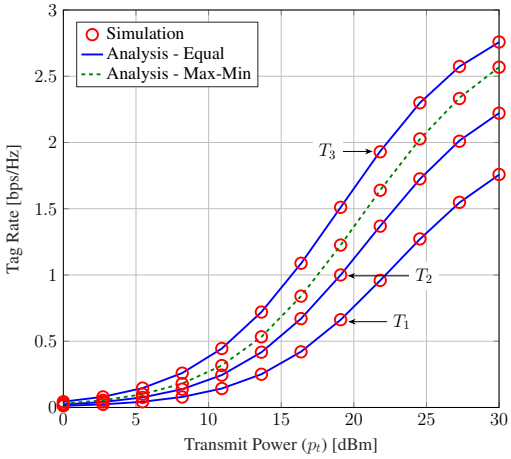

Fig. 3: The tag rate versus transmit power.

As a comparative benchmark, we consider equal power allocation, i.e., $\eta_{mk} = 1/K$ for $m \in \mathcal{M}$ and $k \in \mathcal{K}$. We also plot Monte Carlo simulations and the derived expressions.

Fig. 2 plots the per tag received power as a function of the number of emitters (M) for $p_t = 0$ dBm. The tag activation threshold, p_b, is also plotted to gain insights. From Fig. 2, our findings reveal that using distributed emitters leads to significant macro diversity gains and results in higher power delivery to the tag, surpassing the activation threshold. Additionally, our power allocation strategy allows for tag activation with just 4 emitters, whereas deploying equal power allocation necessitates at least 25 emitters, leading to increased complexity and cost.

Fig. 3 depicts the achieved rate per tag versus the transmit power at the emitters. As observed, with equal power allocation, due to the near-far effects, T_3, which has a better

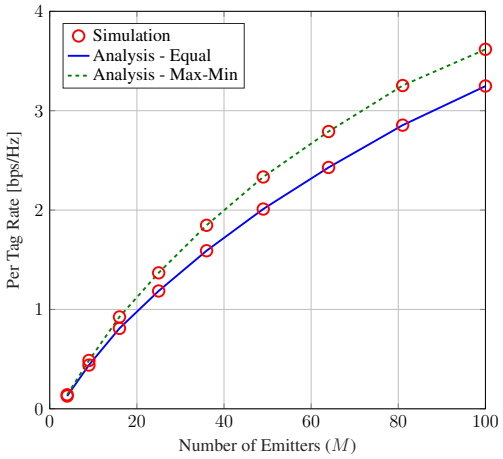

Fig. 4: Per tag rate versus the number of emitters for $p_t = 20$ dBm.

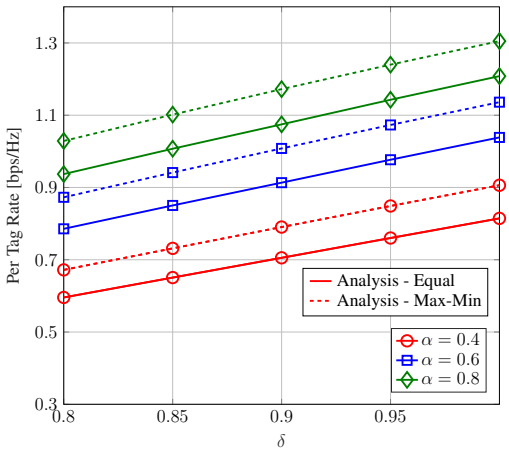

Fig. 5: Per tag rate as a function of imperfect CSI (δ) for $p_t = 20$ dBm .

channel, achieves the highest rate while T_1 with the worst channel achieves the lowest rate, respectively, 2.75 bps/Hz and 1.75 bps/Hz at $p_t = 30$ dBm. On the other hand, our algorithm improves fairness by suppressing the near-far effects. Regardless of the locations of the tags, it thus achieves the maximum possible rate per tag, 2.57 bps/Hz at $p_t = 30$ dBm.

Fig. 4 depicts the achieved per-tag rate as a function of the number of the emitters, with each at $p_t = 20$ dBm. As expected, more emitters lead to a higher rate for each tag, owing to the greater received power. Furthermore, Algorithm 1 outperforms equal power allocation significantly.

It is worth mentioning that some tags, for example, T_3 (Fig. 3), achieve higher rates with equal power allocation than the proposed Algorithm 1. However, due to the near-far effect, equal power allocation may not always guarantee tag activation (Fig. 2). On the other side, the proposed approach eliminates this issue by providing sufficient power to the tags. Therefore, it not only ensures uniform QoS for tags but also tag activation.

We further investigate the effects of CSI errors on the performance of the network in Fig. 5, where the achieved per-tag rate is plotted as a function of δ for different α and $p_t = 20$ dBm. The rate of each tag increases with CSI

estimation quality, and as δ approaches 1, i.e., perfect CSI, the tags achieve higher rates. For $\alpha = 0.8$ and $\delta = 1$, with Algorithm 1, each tag achieves $1.3\,\mathrm{bps/Hz}$, which decreases to $0.28\,\mathrm{bps/Hz}$ for $\delta = 0.8$ (imperfect CSI). Nonetheless, Algorithm 1 outperforms the equal power allocation scheme.

VI. Conclusion

A distributed RF emitter-assisted BiBC setup has been proposed and investigated to improve the EH ability of multiple tags and to reduce their performance dependency on the spatial location. To this end, we optimally allocate power to the emitters to achieve a uniform rate across all tags and to alleviate spatial rate disparities. The use of distributed emitters yields significant benefits, suggesting a promising avenue for future research. Emitter/reader selection techniques can then be employed to establish a green (energy-efficient) BiBC. However, the exchange of CSI among the emitters/readers may increase the front-hauling overhead, which can be resolved through local processing at emitters/readers. The optimal emitter placement problem is a future topic as well.

Appendix A

We first proceed to compute the expectation term in the numerator of (11) as follows:

$$\begin{aligned}
&\mathbb{E}\left\{\left|\mathbf{u}_k^{\mathrm{T}}\mathbf{g}_k\sum\nolimits_{i\in\mathcal{K}}\mathbf{h}_k^{\mathrm{T}}\mathbf{N}_i^{1/2}\mathbf{w}_i\right|^2\right\}\\
&=\sum\nolimits_{m\in\mathcal{M}}\eta_{mk}\mathbb{E}\left\{\left|\hat{\mathbf{g}}_k^{\mathrm{H}}(\hat{\mathbf{g}}_k+\tilde{\mathbf{g}}_k)\right|^2\right\}\\
&\quad\times\mathbb{E}\left\{\left|(\hat{h}_{mk}+\tilde{h}_{mk})\hat{h}_{mk}^*\right|^2\right\}\\
&\quad+\sum\nolimits_{i\in\mathcal{K}_k}\sum\nolimits_{m\in\mathcal{M}}\eta_{mi}\mathbb{E}\left\{\left|\hat{\mathbf{g}}_k^{\mathrm{H}}(\hat{\mathbf{g}}_k+\tilde{\mathbf{g}}_k)\right|^2\right\}\\
&\quad\times\mathbb{E}\left\{\left|(\hat{h}_{mk}+\tilde{h}_{mk})\hat{h}_{mi}^*\right|^2\right\}\\
&\overset{(a)}{=}L\delta^3(L\delta+1)\sum\nolimits_{m\in\mathcal{M}}\eta_{mk}\zeta_{h_{mk}}^2\\
&\quad+L\delta^2(L\delta+1)\sum\nolimits_{m\in\mathcal{M}}\sum\nolimits_{i\in\mathcal{K}}\eta_{mi}\zeta_{h_{mk}}\zeta_{h_{mi}},
\end{aligned}\tag{20}$$

where (a) comes from the fact that, for any vector $\mathbf{z}\sim\mathcal{CN}(\mathbf{0},\theta\mathbf{I}_L)$, we have $\mathbb{E}\left\{|\mathbf{z}^{\mathrm{H}}\mathbf{z}|^2\right\}=(L^2+L)\theta^2$.

Moreover, the first expectation term in the denominator of (11) is calculated as

$$\begin{aligned}
&\mathbb{E}\left\{\left|\mathbf{u}_k^{\mathrm{T}}\mathbf{g}_j\sum\nolimits_{i\in\mathcal{K}}\mathbf{h}_j^{\mathrm{T}}\mathbf{N}_i^{1/2}\mathbf{w}_i s\right|^2\right\}\\
&=\mathbb{E}\left\{\left|\hat{\mathbf{g}}_k^H\mathbf{g}_j\sum\nolimits_{i\in\mathcal{K}}\mathbf{h}_j^{\mathrm{T}}\mathbf{N}_i^{1/2}\hat{\mathbf{h}}_i^*\right|^2\right\}\\
&=\mathbb{E}\left\{\left|\hat{\mathbf{g}}_k^H\mathbf{g}_j\right|^2\right\}\sum\nolimits_{m\in\mathcal{M}}\sum\nolimits_{i\in\mathcal{K}}\eta_{mi}\mathbb{E}\left\{\left|h_{mj}\hat{h}_{mi}^*\right|^2\right\}\\
&=L\delta^3\sum\nolimits_{m\in\mathcal{M}}\eta_{mj}\zeta_{g_k}\zeta_{g_j}\zeta_{h_{mj}}^2\\
&\quad+L\delta^2\sum\nolimits_{m\in\mathcal{M}}\sum\nolimits_{i\in\mathcal{K}}\eta_{mi}\zeta_{g_k}\zeta_{g_j}\zeta_{h_{mi}}\zeta_{h_{mj}}.
\end{aligned}\tag{21}$$

The second expectation term in the denominator of (11) is evaluated as

$$\mathbb{E}\{\|\mathbf{u}_k\|^2\}=\mathbb{E}\{\hat{\mathbf{g}}_k^H\hat{\mathbf{g}}_k\}=L\delta\zeta_{g_k}.\tag{22}$$

By substituting (20), (21), and (22) into (11), the closed-form SINR is derived as in (12).

References

[1] "3GPP TSG RAN Meeting −94e, Study proposal on passive IoT, 8A.1 (from RP-213368)," Dec. 2021. Available Online: https://www.3gpp.org/DynaReport/TDocExMtg--RP-94-e--60214.htm.

[2] D. Galappaththige, F. Rezaei, C. Tellambura, and S. Herath, "Link budget analysis for backscatter-based passive IoT," *IEEE Access*, vol. 10, pp. 128890–128922, Dec. 2022.

[3] F. Rezaei, D. Galappaththige, C. Tellambura, and S. Herath, "Coding techniques for backscatter communications - A contemporary survey," *IEEE Commun. Surveys Tuts.*, pp. 1–1, 2th Quat. 2023.

[4] Ö. Demir, E. Björnson, and L. Sanguinetti, *Foundations of User-Centric Cell-Free Massive MIMO*. Foundations and trends in signal processing, Now Publishers, 2021.

[5] Z. Dai, R. Li, J. Xu, Y. Zeng, and S. Jin, "Cell-free symbiotic radio: Channel estimation method and achievable rate analysis," in *IEEE/CIC Int. Conf. Commun. China (ICCC Workshops)*, pp. 25–30, Jul. 2021.

[6] Z. Dai, R. Li, J. Xu, Y. Zeng, and S. Jin, "Rate-region characterization and channel estimation for cell-free symbiotic radio communications," *IEEE Trans. Commun.*, vol. 71, pp. 674–687, Feb. 2023.

[7] K. Han and K. Huang, "Wirelessly powered backscatter communication networks: Modeling, coverage, and capacity," *IEEE Trans. Wireless Commun.*, vol. 16, pp. 2548–2561, Apr. 2017.

[8] X. Jia and X. Zhou, "Power beacon placement for maximizing guaranteed coverage in bistatic backscatter networks," *IEEE Trans. Commun.*, vol. 69, pp. 7895–7909, Nov. 2021.

[9] H. Yang, Y. Ye, K. Liang, and X. Chu, "Power beacon energy consumption minimization in wireless powered backscatter communication networks," *Early Access*, Apr. 2023.

[10] H. Yang, Y. Ye, and X. Chu, "Max-min energy-efficient resource allocation for wireless powered backscatter networks," *IEEE Wireless Commun. Lett.*, vol. 9, pp. 688–692, May 2020.

[11] K. Shen and W. Yu, "Fractional programming for communication systems—part I: Power control and beamforming," *IEEE Trans. Signal Process.*, vol. 66, pp. 2616–2630, May 2018.

[12] F. Rezaei, D. Galappaththige, C. Tellambura, and A. Maaref, "Time-spread pilot-based channel estimation for backscatter networks," *IEEE Trans. Commun.*, vol. 72, pp. 434–449, Jan. 2024.

[13] S. M. Kay, *Fundamentals of Statistical Signal Processing: Estimation Theory*. USA: Prentice-Hall, Inc., 1993.

[14] D. Galappaththige, F. Rezaei, C. Tellambura, and S. Herath, "RIS-empowered ambient backscatter communication systems," *IEEE Wireless Commun. Lett.*, vol. 12, pp. 173–177, Jan. 2023.

[15] D. Galappaththige and G. Aruma Baduge, "Exploiting distributed IRSs for enabling SWIPT," *IEEE Wireless Commun. Lett.*, vol. 11, pp. 673–677, Apr. 2022.

[16] D. Galappaththige, R. Shrestha, and G. A. Aruma Baduge, "Exploiting cell-free massive MIMO for enabling simultaneous wireless information and power transfer," *IEEE Trans. Green Commun. Netw.*, vol. 5, pp. 1541–1557, Sept. 2021.

[17] Q. Zhang, S. Jin, K.-K. Wong, H. Zhu, and M. Matthaiou, "Power scaling of uplink massive MIMO systems with arbitrary-rank channel means," *IEEE J. Sel. Topics Signal Process.*, vol. 8, pp. 966–981, Oct. 2014.

[18] "3GPP TSG RAN −97e3, Study on ambient IoT , 9.1 (from RP-222685)," Sept. 2022. Available Online: https://portal.3gpp.org/ngppapp/TdocList.aspx?meetingId=60043.

[19] A. Ben-Tal and A. S. Nemirovskiaei, *Lectures on Modern Convex Optimization: Analysis, Algorithms, and Engineering Applications*. USA: Society for Industrial and Applied Mathematics, 2001.

[20] J. S. Borrero, C. Gillen, and O. A. Prokopyev, "Fractional 0—1 programming: Applications and algorithms," *J. of Global Optimization*, vol. 69, pp. 255–282, Sept. 2017.

[21] "3GPP TR 36.814, further advancements for E-UTRA physical layer aspects, V.9.0.0 Rel. 9," Mar. 2010. Available Online: https://portal.3gpp.org/desktopmodules/Specifications/SpecificationDetails.aspx?specificationId=2493.